Power Electronic Systems
Laboratory

IEEE/ASME Transactions on Mechatronics, Vol. 16, No. 3, pp. 431-439, June 2011.

Bearingless Permanent-Magnet Motor with 4/12 Slot-Pole Ratio for Bioreactor Stirring Applications

T. Reichert
T. Nussbaumer
W. Gruber
J. W. Kolar

Eidgenössische Technische Hochschule Zürich
Swiss Federal Institute of Technology Zurich

Bearingless Permanent-Magnet Motor with 4/12 Slot-Pole Ratio for Bioreactor Stirring Applications

Thomas Reichert, *Student Member, IEEE*, Thomas Nussbaumer, *Member, IEEE*, Wolfgang Gruber, *Member, IEEE*, and Johann W. Kolar, *Fellow, IEEE*

***Abstract*—This article presents a novel topology for a bearingless permanent-magnet motor. This disk-shaped motor, featuring an exterior rotor, can be advantageously employed in delicate bioreactor processes. Both torque and bearing forces originate inside this magnetically levitated motor and are generated with concentrated combined windings. Using 3-D-FEM analysis, the optimal machine sizing parameters are evaluated with the goal to maximize torque while providing sufficient bearing forces to allow a precise and stable operation. The results from the sizing optimization and from the force and torque analysis have been implemented and tested with a real-size prototype setup.**

***Index Terms*—Bearingless motor, bioreactor stirring, high torque, large air gap, permanent-magnet synchronous motor (PMSM).**

I. Introduction

IN TECHNOLOGY sectors that ask for highly clean environment and gentle work procedures, a motor with a magnetic bearing can be advantageous over a motor with a conventional bearing despite its higher cost, control effort and machine size [1]–[4]. A compact setup can be achieved with the bearingless motor [5]–[13], because it integrates the magnetic bearing and the drive into a single electromagnetic device. Due to its magnetically levitated rotor, this motor concept is completely free of wear, which guarantees long life time and low maintenance costs. Moreover, it does not suffer from friction and requires no lubrication. Therefore, this motor is highly qualified for the use in processes that take place inside hermetically sealed enclosures such as reactors, pumps, etc. Only the levitated rotor is placed inside the process room, whereas the stator and all the control, sensors, and power electronics are placed outside of the enclosure.

The stirred vessel is the most commonly used type of bioreactor [14]–[20]. One or several agitators create a loop flow inside the vessel, which is necessary to maintain a homogeneous, cell-friendly environment by constantly supplying the cell culture with air bubbles and nutrition. The agitators can either be mounted from the bottom or from the top (requiring a longer shaft). Top-mounting, however, significantly reduces the space for inlets and sensor mountings (e.g., sensors for temperature or pH-value measurements) and requires large head space for assembly work, wherefore in many applications bottom-mounted stirrers are preferred. The main requirement for the motor (agitator) of such a stirred bioreactor is a high torque at usually rather low rotational speeds [15], [18]. State-of-the-art bioreactors often use an external motor with a long rotating shaft passing through a sealed opening in the reactor wall [see Fig. 1(a)]. Usually, a double mechanical seal is employed which leads to a reactor that is not absolutely leakage-proof [19]. Moreover, the seal creates pinch-off areas inside the vessel that harm the cell culture and particles from wear can impact the process quality. In order to avoid the risk of leakage, the torque from an outer motor can alternatively be transmitted by means of a magnetic coupling [see Fig. 1(b)]. However, an additional sliding contact bearing is required within the vessel in order to stabilize the mixing head [19]. Therefore, the problems of pinch-off areas and particle contamination due to wear persist. Alternative agitator concepts (such as the magnetic stirrer [21], [22], which is only suitable for small-scale bioreactors) do not exist for industrial bioreactors of a certain size exceeding some tens of liters of reaction volume.

With an agitator based on the concept of the bearingless motor, the aforementioned drawbacks of the existing agitator concepts could be overcome. A magnetically levitated motor requires no seals and has absolutely no direct contact with the

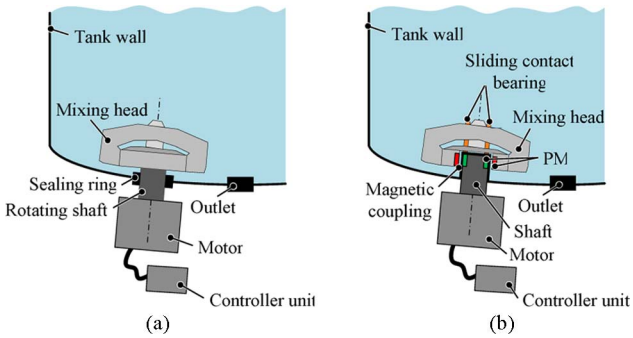

Fig. 1. Schematic view of the lower part of a bioreactor with two different bottom-mounted agitators. The motor in (a) transmits the rotation energy with a rotating shaft through a sealing, whereas the motor in (b) is built with a magnetic coupling and an additional bearing inside the tank.

Manuscript received July 15, 2010; revised November 15, 2010; accepted February 7, 2011. Date of publication April 11, 2011; date of current version May 6, 2011. Recommended by Guest Editor C. H. Menq.

T. Reichert is with the Swiss Federal Insitute of Technology (ETH) Zurich, Power Electronic Systems Laboratory, LEM-AMT, Zurich 8005, Switzerland (e-mail: reichert@lem.ee.ethz.ch).

T. Nussbaumer is with Levitronix GmbH, Zurich 8005, Switzerland (e-mail: nussbaumer@levitronix.com).

W. Gruber is with the ACCM GmbH (Johannes Kepler University Linz), Linz 4040, Austria (e-mail: Wolfgang.Gruber@jku.at).

J. W. Kolar is with the Swiss Federal Institute of Technology (ETH) Zurich, Power Electronic Systems Laboratory, ETL H23, Zurich 8092, Switzerland (e-mail: kolar@lem.ee.ethz.ch).

Color versions of one or more of the figures in this paper are available online at http://ieeexplore.ieee.org.

Digital Object Identifier 10.1109/TMECH.2011.2122340

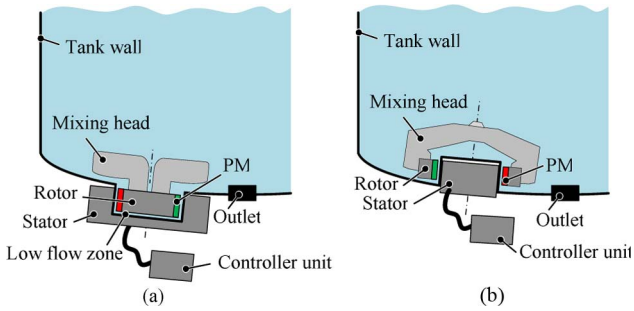

Fig. 2. Schematic view of the lower part of a bioreactor with two single bottom-mounted agitators. In order to avoid pinch-off areas and wear, a bearingless motor is employed. The motor in (a) is built in interior rotor construction, suffering from low flow zones. With an exterior rotor construction (b), an advantageous agitator can be realized.

reactor wall. Therefore, this motor will not suffer from wear and due to low shear forces (avoiding pinch-off areas), the impact on cell destruction can be significantly reduced. Moreover, the large possible fluid gap makes this motor suitable for clean-in-place (CIP) and sterilization-in-place (SIP) applications [23]. Therefore, the goal of this paper is to propose and analyze a new motor concept, which should significantly improve the performance of bioreactor processes.

In this paper, a novel bearingless motor topology, consisting of a disk-shaped exterior rotor with a pole pair number of six and a stator with four stator teeth, is introduced. In Section II, the motor requirements are described and the selection of the motor setup is derived. Section III describes the combined torque and force production of this novel machine. With 3-D magnetostatic FEM simulations, the optimal design is derived in Section IV. Moreover, the optimal winding number per coil is analyzed. Finally, a prototype setup has been built for feasibility studies and verification of the simulations (see Section V).

II. Selection Criteria For Motor Setup

In this paper, the focus lies on a bioreactor with a single bottom-mounted agitator. The outer diameter of the impeller depends on the size of the vessel. For a targeted bioreactor with a volume of 500 l, the outer diameter of the impeller is set to 170 mm. The magnetic gap between stator and rotor needs to be sufficiently large so that the rotor has a certain distance from the reactor wall when levitating. For a wall thickness of 1 mm, the magnetic gap thickness is set to 4 mm so that there is sufficient physical space between the wall and the rotor during operation. This is necessary to avoid pinch-off areas and for the CIP and SIP processes.

In a first step, the selection between interior and exterior rotor type motor has to be made. Fig. 2 compares the two concepts. In case of an interior rotor setup [see Fig. 2(a)], the vessel is extended at the bottom so that the rotor can be placed inside and the stator around it. The impeller has to be fixed on top of the rotor so that the impeller blades can be mounted higher inside the vessel allowing a higher agitation impact. However, this interior rotor setup bears a significant disadvantage. The flow will only slightly enter the extended bottom area, thus, creating an undesired dead zone. Moreover, the required impeller impairs the stability of the magnetic bearing. Therefore, the exterior rotor type [see Fig. 2(b)] has been selected. It consists of an indentation at the bottom of the vessel, where the disk-shaped stator is placed. The hollow rotor ring is then placed around it inside the vessel. This setup allows a flexible impeller design and guarantees sufficient flow within the whole vessel. This new concept can be understood as a further improvement of a magnetic coupling. Additionally to the torque transmission by means of magnetic forces, radial bearing forces are generated as well and transmitted through the reactor wall, which allows abandoning any sliding contact bearings within the reactor.

In a next step, the number of stator teeth and the pole pair number have to be chosen. The outer diameter of the motor depends on the type of impeller. For the exterior rotor type, the impeller blades are directly mounted at the outer part of the rotor [see Fig. 2(b)]. The minimum blade length required is set to 20 mm, thus, the outer diameter of the motor is limited to 130 mm. This implies that for this experimental setup the available space for the stator will be rather restricted, since it needs to be placed inside the hollow rotor ring. Therefore, only a setup with a small number of stator teeth is recommendable, since otherwise there is not enough space for the stator windings. Sufficient winding space yet is required, since the torque directly depends on the coil current (see Section III) and a certain maximum current density shall not be exceeded. The minimum number of coils for a bearingless motor is four, thus, at least four stator teeth are needed. The drive of such a setup would show single-phase characteristics and comparably large cogging torque. Setups with five or more stator teeth would also be possible. A stator with five teeth would have almost zero cogging torque. However, the setup with five stator teeth results in unbalanced passive bearing forces, thus, high control currents are required. Moreover, a computationally intensive control would have to be implemented in order to generate smooth levitation of the rotor and torque independently of the actual rotor angle. Further setups with six or more stator teeth already limit the winding space significantly so that they are not considered for the proposed reactor dimensions. However, they could be an interesting alternative for larger reactor volumes. These considerations lead to the selection of a motor with four stator teeth despite its aforementioned disadvantages. With a pole pair number of six, this setup can produce both torque and bearing forces with only four coils, as will be described in the next section.

III. Torque and Bearing Forces

The motor setup was defined to feature an exterior rotor with a pole pair number of six and a stator teeth number of four. The rotor consists of 12 permanent magnets that are radially magnetized in alternating order (see Fig. 3). Four concentrated stator coils (one per stator tooth) have to produce both torque and bearing forces. Each coil can produce a radial force (often referred to as Maxwell force) and a tangential force (often referred to as Lorentz force). The right combination of these forces then allows to combine drive and bearing in one stator [24]. The required current excitation can be examined separately for torque

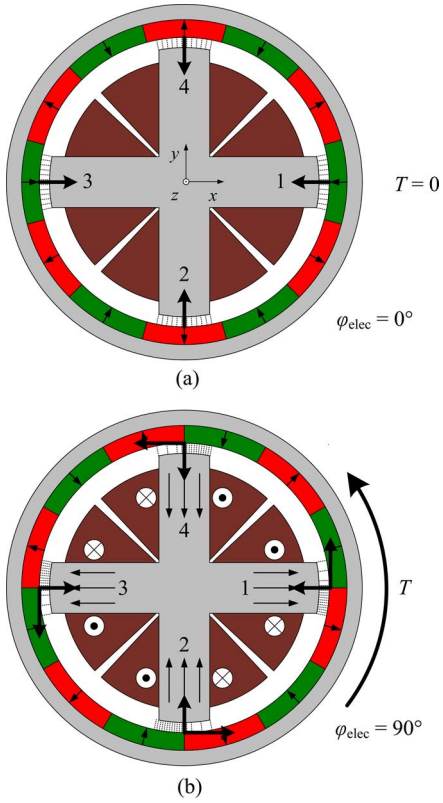

Fig. 3. Excitation currents for torque generation and the resulting radial and tangential forces. For the rotor position in (a), only radial forces can be generated so that no torque output will result. If the rotor is turned by 90 electrical degrees (b), tangential forces are created as well, which sum up to the peak torque at this position.

and bearing forces and will be superimposed in the control commands. This concept of combined coils (no separate drive and bearing coils) is advantageous in terms of reducing the total required current, thus, reducing copper losses [25].

The control algorithm for both torque and bearing forces requires permanent knowledge about the angular position of the rotor. Therefore, Hall-effect sensors measure the magnetic field of the rotor in order to determine its position. This angular position is measured in the unit of an electrical angle, which is defined as the product of the mechanical rotor angle times the pole pair number p

$$\varphi_{\mathrm{elec}} = p \cdot \varphi_{\mathrm{mech}}. \tag{1}$$

A. Motor Torque

This motor topology shows single-phase characteristics, thus, there is a position where no torque can be produced [see Fig. 3(a)]. In this angular position ($\varphi_{\mathrm{elec}} = 0°$), there is always a full magnet facing a stator tooth. If any of the coils would be excited, only radial forces would result that would move the rotor in the xy-plane, but no torque generation is possible. In the other specific case [for $\varphi_{\mathrm{elec}} = 90°$ in Fig. 3(b)] only tangential forces can be produced when the coils are excited, since the stator teeth face two magnets equally. Therefore, the torque output is maximal for this constellation.

For the control over the whole angular range, the four stator coils have to be fed with a sinusoidal excitation current being in-phase with the electrical angle. Two opposite coils are in-phase, whereas they are phase-shifted by 180° with the remaining two coils, thus, leading two a rotating magnetic field with twice the mechanical rotational frequency. Together with the harmonics generated by the four stator teeth, a stator field with pole pair number of six results [26]. All four coils then produce radial forces that annihilate each other. However, the tangential forces result in a motor torque, which oscillates with the square value of a sine wave when rotating with a sinusoidal drive current. For a torque-current factor $k_{\mathrm{I,Tn}}$ of one coil, the number of windings per coil N_{coil} and the peak value of the drive current $\hat{I}_{\mathrm{drv}}$ in one coil, the overall motor torque is given by

$$T_{\mathrm{ac}}(\varphi_{\mathrm{elec}}) = 4 \cdot k_{\mathrm{I,Tn}} \cdot \sin^2(\varphi_{\mathrm{elec}}) \cdot N_{\mathrm{coil}} \cdot \hat{I}_{\mathrm{drv}}. \tag{2}$$

The average torque output is then exactly 50% of the peak torque output occurring when $\varphi_{\mathrm{elec}} = 90°$. For a maximum allowed rms value of the current $I_{\mathrm{drv,rms}}$, the average torque is limited to

$$T_{\mathrm{ac,avg}} = 2 \cdot \sqrt{2} \cdot k_{\mathrm{I,Tn}} \cdot N_{\mathrm{coil}} \cdot I_{\mathrm{drv,rms}}. \tag{3}$$

Alternatively, the coils could be excited with dc current with commutation for $\varphi_{\mathrm{elec}} = 0°$ and $\varphi_{\mathrm{elec}} = 180°$, respectively. The torque of this brushless dc variant would become

$$T_{\mathrm{dc}}(\varphi_{\mathrm{elec}}) = 4 \cdot k_{\mathrm{I,Tn}} \cdot |\sin(\varphi_{\mathrm{elec}})| \cdot N_{\mathrm{coil}} \cdot \hat{I}_{\mathrm{drv}}. \tag{4}$$

The average torque output is then $2/\pi = 63.7\%$ of the peak torque output occurring when $\varphi_{\mathrm{elec}} = 90°$. For this dc variant, however, the amplitude of the drive current is equal to its rms value. Thus, the torque is limited to

$$T_{\mathrm{dc,avg}} = \frac{8}{\pi} \cdot k_{\mathrm{I,Tn}} \cdot N_{\mathrm{coil}} \cdot I_{\mathrm{drv,rms}}. \tag{5}$$

When comparing the average torque

$$\frac{T_{\mathrm{ac,avg}}}{T_{\mathrm{dc,avg}}} = 2 \cdot \sqrt{2} \cdot \frac{\pi}{8} = 1.11 \tag{6}$$

it can be seen that for dc excitation, the average torque is 11% smaller for the same rms value of the current. Moreover, due to the alternating bearing currents, there is no simplification if dc drive current was used, since the currents are superimposed in each stator coil. For these reasons, only sinusoidal excitation will be considered for the control.

This motor setup provokes a cogging torque that interferes with the active motor torque. Fig. 4 shows the cogging torque in dependence on the angular position. It can be seen that there are two stable positions where the rotor would stop when no drive current is applied. These two positions happen to occur at the very same electrical angle where maximum torque can be achieved. Moreover, there is an unstable working point at the angular position where no torque can be generated. Any slight angular displacement would lead to a cogging torque that would accelerate the rotor. Therefore, even though this motor shows single-phase characteristics for the drive, it will always be possible to start the rotation and to run it continuously. However, the influence of the cogging torque can be seen at very low

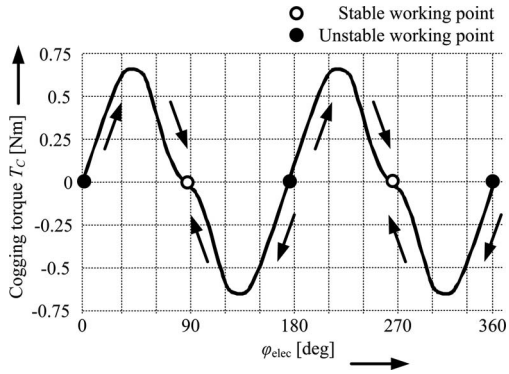

Fig. 4. Cogging torque of the motor in dependence on the electrical angle, when no excitation current is applied, based on the optimal design (see Section IV). There are two stable working points where the rotor would come to standstill. For these two specific angles (90° and 270°), maximum torque can be produced. Therefore, the rotation can always start and run despite the single-phase drive characteristics.

speeds, where the rotation will be jerky. For higher speeds, this influence will vanish. Additionally, the influence of the cogging torque could be further decreased by slight topology modifications that disturb the symmetry or by temporarily displacing the rotor from its center position.

B. Bearing Forces

The rotor of the bearingless motor has to be stabilized in six degrees of freedom. One degree of freedom is the rotation that is controlled with the drive currents. Therefore, the magnetic bearing has to stabilize the five remaining degrees of freedom. With the ring-shaped rotor type, only the radial displacements in x- and y-direction have to be controlled actively by applying bearing currents. The other three degrees of freedom (tilting and axial displacement) are stabilized passively [13].

1) Passive Bearing Forces: Both axial and tilting deflections are stabilized passively by means of attracting reluctance forces. The rotor weight m_R counteracts the axial force, thus, this reluctance force has to be sufficiently high so that the rotor position is only lowered up to a moderate extent (Δz). Therefore, the requirement for the axial stiffness factor k_z can be stated as

$$k_z > \frac{m_R \cdot g}{\Delta z} \tag{7}$$

where g is the gravitational acceleration constant ($g = 9.81\ \mathrm{m/s^2}$).

The tilting mainly depends on the ratio of motor diameter to machine length (or height, respectively). A sufficient reluctance force against tilting disturbance is a key requirement for the proper functioning of the bearingless motor. It is obvious that for a fixed rotor setup, these reluctance forces grow with the available stator iron area that the permanent magnets can act on. From this point of view, it would be recommendable to enlarge the tooth tip opening angle (see Section IV).

2) Active Bearing Forces: The remaining two degrees of freedom regulate the radial position of the rotor. There are also passive reluctance forces acting in radial direction, yet they do not have a stable working point. When the rotor is slightly

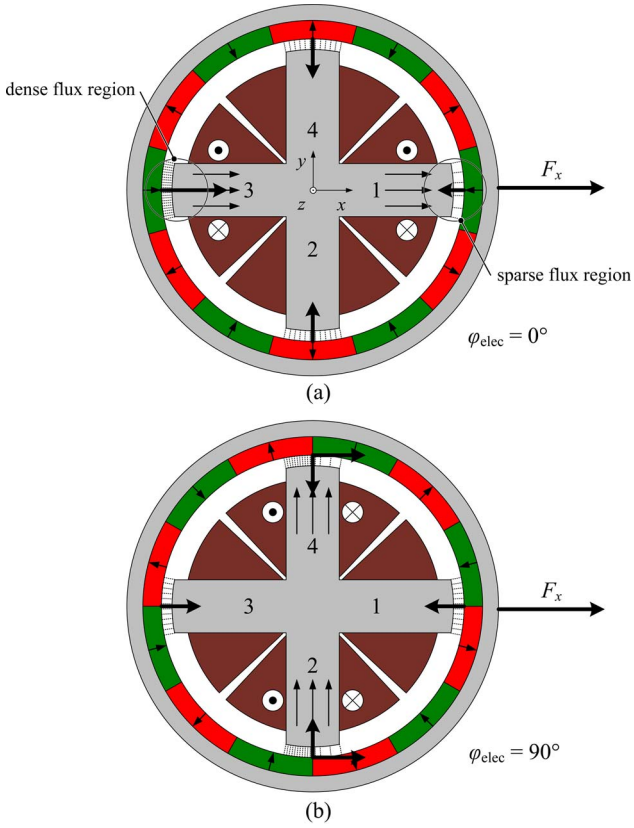

Fig. 5. Excitation currents for the force generation in positive x-direction and the resulting radial and tangential forces. For the rotor position in (a), only radial forces can be generated so that the resulting radial force is generated by the coils 1 and 3. For the other specific angular position (b), the sum of the tangential forces generated by coils 2 and 4 results in a radial force.

displaced from its center position, the radial reluctance forces become stronger on the side where the magnetic gap is now smaller. Thus, the rotor is removed even further away from its center position until it touches the stator. Therefore, the radial displacement has to be regulated permanently with an active control. The bearing system consists of two separate phases that are shifted by 90°. Each phase itself consists of two opposite coils, whereas these coils are phase shifted by 180°, thus, leading two a rotating magnetic field with the mechanical rotational frequency. Together with the harmonics generated by the four stator teeth, a stator field with pole pair number of five results [26]. As depicted in Fig. 5(a) and (b), such a coil arrangement (current feed shown for force generation in x-direction) does not create torque, but bearing forces in x- (or alternatively in y-) direction that depend on the rotor angle. For the two directions

$$F_x(\varphi_{\mathrm{elec}}) = \begin{array}{l} k_{\mathrm{I,Fr}} \cdot \cos(\varphi_{\mathrm{elec}}) \cdot N_{\mathrm{coil}} \cdot I_{\mathrm{bng},1,x}(\varphi_{\mathrm{elec}}) \\ -k_{\mathrm{I,Ft}} \cdot \sin(\varphi_{\mathrm{elec}}) \cdot N_{\mathrm{coil}} \cdot I_{\mathrm{bng},2,x}(\varphi_{\mathrm{elec}}) \\ -k_{\mathrm{I,Fr}} \cdot \cos(\varphi_{\mathrm{elec}}) \cdot N_{\mathrm{coil}} \cdot I_{\mathrm{bng},3,x}(\varphi_{\mathrm{elec}}) \\ +k_{\mathrm{I,Ft}} \cdot \sin(\varphi_{\mathrm{elec}}) \cdot N_{\mathrm{coil}} \cdot I_{\mathrm{bng},4,x}(\varphi_{\mathrm{elec}}) \end{array} \tag{8}$$

and

$$F_y(\varphi_{\mathrm{elec}}) = \begin{array}{l} k_{\mathrm{I,Ft}} \cdot \sin(\varphi_{\mathrm{elec}}) \cdot N_{\mathrm{coil}} \cdot I_{\mathrm{bng},1,y}(\varphi_{\mathrm{elec}}) \\ +k_{\mathrm{I,Fr}} \cdot \cos(\varphi_{\mathrm{elec}}) \cdot N_{\mathrm{coil}} \cdot I_{\mathrm{bng},2,y}(\varphi_{\mathrm{elec}}) \\ -k_{\mathrm{I,Ft}} \cdot \sin(\varphi_{\mathrm{elec}}) \cdot N_{\mathrm{coil}} \cdot I_{\mathrm{bng},3,y}(\varphi_{\mathrm{elec}}) \\ -k_{\mathrm{I,Fr}} \cdot \cos(\varphi_{\mathrm{elec}}) \cdot N_{\mathrm{coil}} \cdot I_{\mathrm{bng},4,y}(\varphi_{\mathrm{elec}}) \end{array} \tag{9}$$

hold true, with the force-current factors per coil in radial and tangential direction $k_{\mathrm{I,Fr}}$ and $k_{\mathrm{I,Ft}}$, respectively, the number of windings per coil N_{coil}, and the bearing currents per coil $I_{\mathrm{bng},1,\ldots,4,x}$ and $I_{\mathrm{bng},1,\ldots,4,y}$. In Fig. 5(a), the center of the right stator teeth faces the center of one magnet. In order to produce a force in the positive *x*-direction, the field on the right side has to be weakened, whereas it has to be fortified on the left side. Thus, the radial forces are used to center the rotor, whereas the tangential forces are zero in this angular rotor position. In (8), the contribution of these radial force parts is considered with the terms in lines 1 and 3 [lines 2 and 4 in (9) for force generation in *y*-direction]. For an electrical angle of 90°, the centers of the stator teeth face exactly the connection of two magnets [see Fig. 5(b)]. Both radial and tangential forces are created and their superposition results in a force in *x*-direction. The contribution of these force parts is considered in (8) with the terms in lines 2 and 4 and in (9) with the terms in lines 1 and 3.

With all four coils together, bearing forces in every desired radial direction can be generated for every possible angular rotor position. Displacement sensors determine the radial rotor position and feed it to the control algorithm. For a given required force, this control algorithm then calculates the bearing currents in dependence on the angular rotor position. Moreover, these currents depend on the ratio of the two force-current factors. For the generation of a desired force in *x*-direction $\tilde{F}_x$, which is independent of the angular position, the coil currents have to be set to

$$\begin{pmatrix} I_{\mathrm{bng},1,x} \\ I_{\mathrm{bng},2,x} \\ I_{\mathrm{bng},3,x} \\ I_{\mathrm{bng},4,x} \end{pmatrix} = \begin{pmatrix} k_{\mathrm{I,Fr}} \cdot \cos\left(\varphi_{\mathrm{elec}}\right) \\ -k_{\mathrm{I,Ft}} \cdot \sin\left(\varphi_{\mathrm{elec}}\right) \\ -k_{\mathrm{I,Fr}} \cdot \cos\left(\varphi_{\mathrm{elec}}\right) \\ k_{\mathrm{I,Ft}} \cdot \sin\left(\varphi_{\mathrm{elec}}\right) \end{pmatrix} \cdot f\left(\varphi_{\mathrm{elec}}\right) \cdot \frac{\tilde{F}_x}{N_{\mathrm{coil}}} \tag{10}$$

with a weighting factor *f* of

$$f\left(\varphi_{\mathrm{elec}}\right) = \frac{1}{2} \cdot \frac{1}{k_{\mathrm{I,Fr}}^2 \cdot \cos^2\left(\varphi_{\mathrm{elec}}\right) + k_{\mathrm{I,Ft}}^2 \cdot \sin^2\left(\varphi_{\mathrm{elec}}\right)}. \tag{11}$$

The bearing currents for the generation of a force in *y*-direction can be derived accordingly. If the bearing currents are applied according to (10), the drive is not influenced by the forces of the bearing.

The active radial forces have to overcome the destabilizing radial stiffness (with factor k_r) in dependence on the maximal displacement $\Delta r_{\max}$. When respecting a maximally producible radial force $F_{\max}$, the required condition for both directions can be stated as

$$k_{F,\mathrm{overall}}(k_{\mathrm{I,Fr}}, k_{\mathrm{I,Ft}}, \varphi_{\mathrm{elec}}) > \frac{k_r \cdot \Delta r_{\max}}{F_{\max}}. \tag{12}$$

C. Motor Control

Up to now, the torque and force generation have been looked at separately. Moreover, the force generation has been split into a force generation in *x*-direction, as well as in *y*-direction. In order to control all three active degrees of freedom separately, three coils per stator tooth would become necessary. However, there would always be at least one stator tooth where the three coils produce forces that counteract each other. Thus, the sum of the three coil currents would be large even though the resulting force is low. For this reason, the concept of combined windings is applied. This means that only one coil is mounted onto each stator tooth and it produces the forces for both drive and bearing. The required bearing and drive currents are calculated in the digital control and then superimposed mathematically prior to applying them to the stator coil. Additionally, the inverse mathematical transformation has to be undertaken when the coil currents are measured in order to split it into the three degrees again to guarantee an independent control. This concept with a more sophisticated control reduces the assembly work (only one coil per stator tooth) and leads to an optimized power balance [25].

Since the four coils need to be excited with nonsinusoidal currents and independently of each other, the power electronics of the motor have to consist of four full bridges, which are all fed by a dc-link voltage. Each coil is then connected to one of the full bridges and excited individually.

IV. Design And Optimization

Initial selection criteria have already defined the rough design parameters of the new motor topology. With 3-D magnetostatic FEM simulations the optimal shape of the bearingless motor will be evaluated. The goal is to maximize the available torque for mixing, to reduce the cogging torque so that it is not dominating, and to achieve sufficient bearing forces (passively and actively). In a second step, the criteria for the optimal winding number will be derived.

A. Optimization Using 3-D FEM

The geometrical design parameters of the motor are depicted in Fig. 6. The rotor consists of permanent magnets and a back iron ring. Therefore, the optimal thickness of these two elements (δ_{PM} and δ_{BI}, respectively) has to be found. Moreover, this selection determines the diameter of the stator, because it has to be placed entirely within the hollow rotor ring, respecting the required magnetic gap thickness. For the stator, the main parameters are the tooth width w_t, the tooth tip opening angle α_{tt} and the tooth tip thickness d_{tt}. The derivation of the optimal design parameters for such a topology and the influence of the aforementioned variables are described in [27] in great detail.

In summary, the optimal design parameters are mainly influenced by the tradeoff between achieving large magnetomotive force and avoiding heavy saturation. For a large output torque, large magnets and large magnetomotive force (requiring large windings) are advantageous. However, this drastically limits the available space for stator iron, which has a negative effect on the magnetic properties (magnetic saturation is reached with lower magnetomotive force). Consequently, an optimal stator tooth width has to be found, for which an optimal flux-linkage with the magnets can be achieved, while still leaving sufficient slot space that can be filled up with windings. Interestingly, it was found that bar shaped stator teeth without a tooth tip are optimal, which also holds true for magnetically levitated interior rotor motors [28], [29]. Concerning the rotor, the magnet and back iron thickness cannot be excessive, because it would reduce the

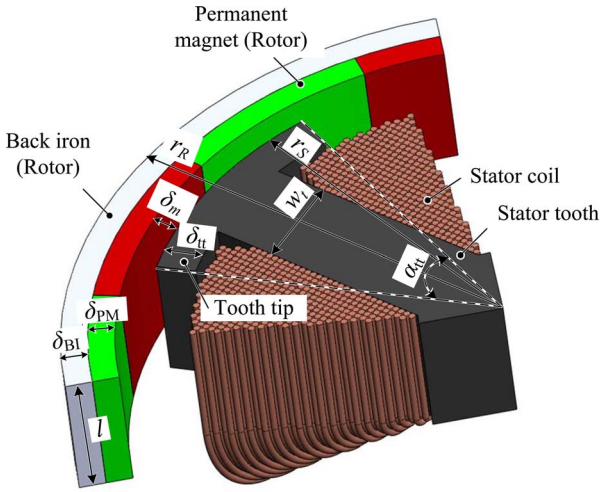

Fig. 6. A single stator tooth of the motor with its design parameters.

TABLE I
OPTIMAL DESIGN PARAMETER AND RATED VALUES

Parameter	Symbol	Value
Number of stator teeth	q	4
Pole pair number	p	6
Outer rotor diameter	d_R	130 mm
Magnetic gap thickness	δ_m	4 mm
Machine length	l	40 mm
Magnet thickness	δ_{PM}	4 mm
Back iron thickness	δ_{BI}	4 mm
Outer stator diameter	d_S	106 mm
Stator tooth width	w_t	15 mm
Winding number	N_{coil}	225
Rated peak torque	$\hat{T}$	8 Nm
Rated average torque	T	4 Nm
Peak cogging torque	T_C	0.7 Nm
Rated speed	n	500 r/min
Rated drive current	$I_{drv,rms}$	5.65 A

available stator and winding space. Moreover, the inner rotor radius (thus, the lever arm) gets enlarged for smaller magnet thickness.

The optimal design parameters found with the 3-D-FEM simulations are summarized in Table I.

B. Optimal Winding Number Per Coil N_{coil}

There is a tradeoff for the optimal winding number per coil N_{coil} between the production of torque and force and dynamic considerations of the bearing.

According to (2), (8), and (9) the production of torque and force would require a large winding number in order to limit the required currents. However, (2), (8), and (9) are only valid as long as no heavy saturation in the iron parts occurs. Therefore, there is an upper limitation for the winding number that avoids the saturation of the iron parts. In addition, there is also an upper limitation considering the dynamic range of the bearing. For these dynamic considerations, the electrical response time (τ_E) and the mechanical time constant (τ_M) have to be compared. The mechanical characteristic time constant according to [6] and [11] depends on the rotor mass m_R and the radial stiffness

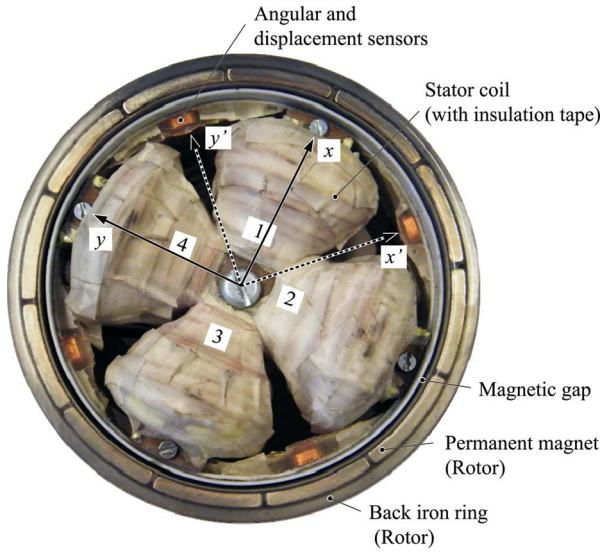

Fig. 7. Prototype of the novel motor for bioreactor stirring applications. The measurement of the position leads to a coordinate system x' and y'. In order to align it with the coils and their force generation, it is shifted by 45°, leading to the new coordinate system with x and y.

factor k_r. For the prototype motor (see Section V), this is

$$\tau_M = \sqrt{\frac{m_R}{k_r}} = \sqrt{\frac{0.975\ \mathrm{kg}}{25000\ \mathrm{N/m}}} = 6.25\,\mathrm{ms}. \tag{13}$$

The maximum electrical response time, given by

$$\tau_E = \frac{\hat{I}_{\mathrm{bng}} \cdot L_{\mathrm{coil}}}{U_{\mathrm{dc}}} = \frac{8\ \mathrm{A}}{48\ \mathrm{V}} \cdot L_{\mathrm{coil}} \tag{14}$$

with the peak value of the bearing current $\hat{I}_{\mathrm{bng}}$, the inductance L_{coil} of the coil, and the dc link voltage U_{dc} (for bearing coils driven by an inverter in full bridge configuration, assuming a maximum duty cycle of 1), must be smaller than τ_M in order to achieve a stable bearing control. Therefore, from the viewpoint of control dynamics, a small value for N_{coil} is preferable considering that L_{coil} scales quadratically with N_{coil}. For a winding number of 225, the coil inductance is 13 mH for the motor at hand. Hence, the electrical time constant becomes 2.2 ms, which is smaller than the mechanical time constant.

V. EVALUATION WITH PROTOTYPE SETUP

The optimal design topology has been implemented in a prototype setup in order to prove the proper functioning of this new motor concept.

A. Experimental Setup

Fig. 7 shows a prototype setup of the proposed topology. The four stator coils produce both torque and bearing forces. In order to operate the motor independently of the actual rotor angle, each of the four coils needs to be controlled individually. In Fig. 8, the employed power electronic converter is depicted. It consists of four full bridges, each of them fed by the dc-link voltage, and each coil is connected to one of these full bridges. Moreover, the current in each of these full-bridges is measured

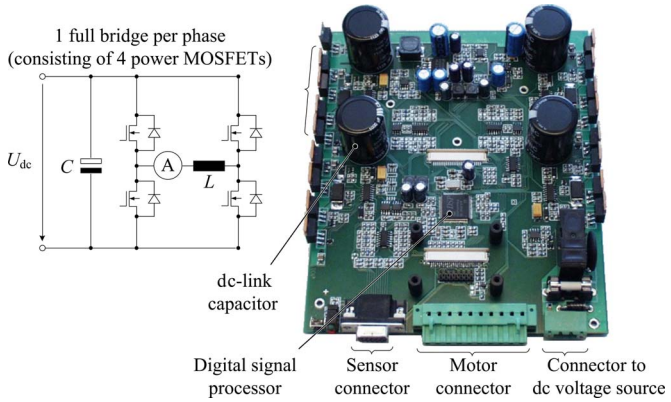

Fig. 8. Picture of the employed power electronic converter. It is fed by a dc voltage of 48 V, which charges the dc-link capacitors. Each of the four coils of the motor is connected to one of the full bridges.

constantly. Additionally, permanent information about the rotor position in radial direction as well as about the angular position is mandatory. The radial rotor position can be measured with any kind of contactless distance sensor (e.g., inductive or eddy-current principle), whereas the rotation angle is usually measured with Hall effect type sensors. All signals from the various sensors are filtered and digitalized before they are fed to the DSP, a TMS320F2811 from Texas Instruments, with a sampling rate of 17.5 kHz. The controller is directly connected to a dc voltage source of 48 V (not shown in Fig. 8), which is the nominal dc-link voltage.

B. Experimental Results

Fig. 9 shows measurements with the prototype during a test operation. In Fig. 9(a), the rotor is turning with rated speed but without any load torque (except air friction, which is very low). In Fig. 9(b), the motor has to overcome an average load torque of about 2.5 Nm (using a mechanical test stand with brake shoes) and the rotational speed is 220 rpm. It can be seen that in both cases, the radial position is very stable, resulting in rotor displacements smaller than 100 μm. Additionally, the currents of two opposing coils (here 1 and 3) are measured using a current probe. Since each coil current is composed of bearing and drive parts, a mathematical separation needs to be undertaken first. The actual bearing current can be calculated by subtracting the two opposing coils (see Section III). It can be seen that the required bearing current is comparably small. During operation without load torque [Fig. 9(a)], the drive current (also calculated from the two coil currents using addition) is low, too, as it only needs to overcome the cogging torque (plus air friction and iron losses, which are both very small). Consequently, it is considerably larger if additional torque is applied [Fig. 9(b)]. The sinusoidal form of the drive current is distorted by the cogging torque, yet a very smooth rotation is achieved in both cases.

As described in Section IV, an important goal of the motor design is the reduction of the cogging torque. However, a certain cogging torque is acceptable for the benefit of achieving a larger motor torque, given that the two design goals might con-

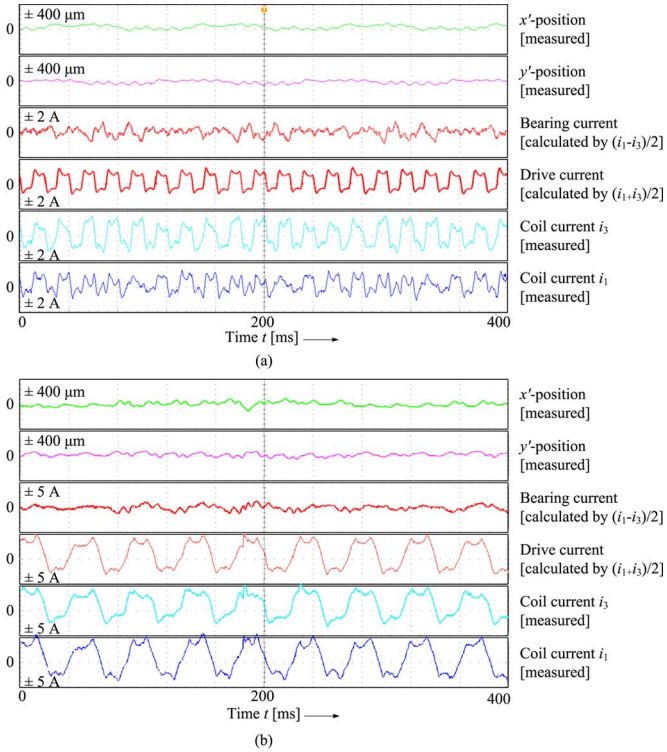

Fig. 9. Measurements with the prototype setup during operation at rated speed without load (a), and with additional load torque of 2.5 Nm (mechanically impressed) while rotating with 220 rpm (b). The rotor position only displaces in a small range from the center (within 100 μm) and only a small bearing current (calculated from the measurements of two opposite coil currents) is required in both cases. The drive current (also calculated from two opposite coil currents) has to overcome the cogging torque in (a), whereas it is obviously larger when additional load torque is applied in (b). (Current scales: 2 A/div. (a) and 5 A/div. (b), position scales: 400 μm/div., time scale: 40 ms/div.)

tradict each other. In any case, even a distorted drive current can never impair the levitation, since the drive forces cannot generate any resulting radial force on the rotor per definition (see Section IIIA), which is additionally confirmed with the experimental analysis.

In Fig. 10, an active displacement of the rotor into the positive y-direction for 400 μm is shown. The x-position is completely decoupled and not affected. The required bearing current is calculated from the measurements of the current in the coils 1 and 3.

C. Motor Efficiency

During operation, losses appear in the stator, the rotor and in the power electronic converter. For the latter, the efficiency can be optimized independently of the actual motor design if the operating values are known. As for the motor losses, they can be subdivided into ohmic copper, eddy current and hysteresis losses. For the targeted rotational speed, the occurring losses due to hysteresis and eddy currents are insignificantly small if the steel of the stator and the rotor back iron is laminated [30]. Consequently, the notable losses result in the stator windings because of the ohmic resistance of the copper. For the prototype setup, the resistance of one coil is 0.65 Ω. In case of rated

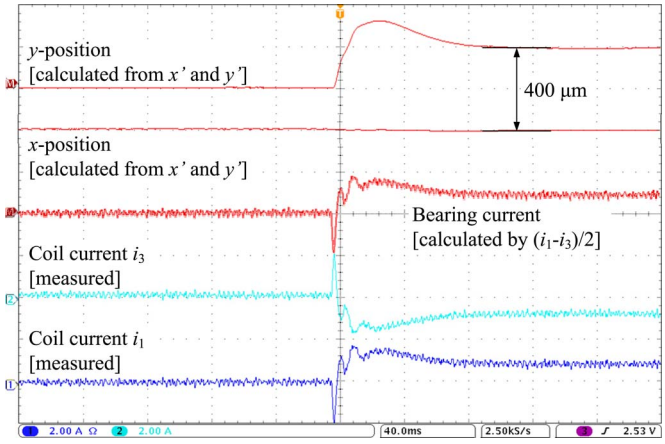

Fig. 10. Measurements of two coil currents and the radial position. A radial displacement step of 400 μm is shown. The bearing current can quickly control the new position. The other radial direction is unaffected. (Current scales: 2 A/div., position scales: 400 μm/div., time scale: 40 ms/div.)

operation, the losses are given by

$$P_{\mathrm{Cu}} = 4 \cdot R_{\mathrm{Cu}} \cdot I^2_{\mathrm{drv,rms}} = 83\,\mathrm{W}. \tag{15}$$

The influence of the bearing has been neglected, since the bearing currents are expected to be low for typical bioreactor operations [see Fig. 9(b)]. Moreover, due to the combined windings, the bearing currents overlap with the drive currents in two of the coils, whereas they suppress each other in the remaining two coils. This means that even for larger bearing currents, the total copper losses would only grow slowly. The mechanical power of the motor is given by

$$P_{\mathrm{rot}} = T \cdot 2\pi n = 210\,\mathrm{W}. \tag{16}$$

Therefore, the efficiency of this prototype for rated torque becomes

$$\eta = \frac{P_{\mathrm{rot}}}{P_{\mathrm{rot}} + P_{\mathrm{Cu}}} = 72\%. \tag{17}$$

Obviously, the winding area was not optimally used for this prototype setup (see Fig. 7). Hence, the copper resistance could still be reduced, which would lead to a significant improvement of the motor efficiency to about 80%, which is a good value considering the large mechanical gap.

VI. Conclusion

A novel motor topology with an exterior ring-shaped rotor with a pole pair number of six and a stator with four stator teeth has been introduced. Concentrated, combined windings, driven by a sophisticated control, allow the generation of both motor torque and bearing forces in a very compact setup. Due to the absence of wear, friction and any lubrication, this motor is especially suitable for delicate bioreactor stirring applications.

References

[1] S.-L. Chen and C.-C. Weng, "Robust Control of a voltage-controlled three-pole active magnetic bearing system," *IEEE/ASME Trans. Mechatronics*, vol. 15, no. 3, pp. 381–388, Jun. 2010.

[2] S.-H. Park and C.-W. Lee, "Decoupled control of a disk-type rotor equipped with a three-pole hybrid magnetic bearing," *IEEE/ASME Trans. Mechatronics*, vol. 15, no. 5, pp. 793–804, Oct. 2010.

[3] C. Weisbacher, H. Stelzer, and K. Hameyer, "Application of a tubular linear actuator as an axial magnetic bearing," *IEEE/ASME Trans. Mechatronics*, vol. 15, no. 4, pp. 615–622, Aug. 2010.

[4] G. R. Jayanth and C.-H. Menq, "Modeling and design of a magnetically actuated two-axis compliant micromanipulator for nanomanipulation," *IEEE/ASME Trans. Mechatronics*, vol. 15, no. 3, pp. 360–370, Jun. 2010.

[5] H. Grabner, W. Amrhein, S. Silber, and W. Gruber, "Nonlinear feedback control of a bearingless brushless DC motor," *IEEE/ASME Trans. Mechatronics*, vol. 15, no. 1, pp. 40–47, Feb. 2010.

[6] T. Schneeberger, T. Nussbaumer, and J. W. Kolar, "Magnetically levitated homopolar hollow-shaft motor," *IEEE/ASME Trans. Mechatronics*, vol. 15, no. 1, pp. 97–107, Feb. 2010.

[7] H. Sugimoto, K. Kamiya, R. Nakamura, J. Asama, A. Chiba, and T. Fukao, "Design and basic characteristics of multi-consequent-pole bearingless motor with Bi-tooth main poles," *IEEE Trans. Magn.*, vol. 45, no. 6, pp. 2791–2794, Jun. 2009.

[8] K. Raggl, B. Warberger, T. Nussbaumer, S. Burger, and J. W. Kolar, "Robust angle-sensorless control of a PMSM bearingless pump," *IEEE Trans. Ind. Electron.*, vol. 56, no. 6, pp. 2076–2085, Jun. 2009.

[9] S.-M. Yang and M.-S. Huang, "Design and implementation of a magnetically levitated single-axis controlled axial blood pump," *IEEE Trans. Ind. Electron.*, vol. 56, no. 6, pp. 2213–2219, Jun. 2009.

[10] S. Zhang and F. L. Luo, "Direct control of radial displacement for bearingless permanent-magnet-type synchronous motors," *IEEE Trans. Ind. Electron.*, vol. 56, no. 2, pp. 542–552, Feb. 2009.

[11] P. Karutz, T. Nussbaumer, W. Gruber, and J. W. Kolar, "Novel magnetically levitated two-level motor," *IEEE/ASME Trans. Mechatronics*, vol. 13, no. 6, pp. 658–668, Dec. 2008.

[12] T. Tera, Y. Yamauchi, A. Chiba, T. Fukao, and M. A. Rahman, "Performance of bearingless and sensorless induction motor drive based on mutual inductances and rotor displacements estimation," *IEEE Trans. Ind. Electron.*, vol. 53, no. 1, pp. 187–194, Feb. 2006.

[13] R. Schoeb and N. Barletta, "Principle and application of a bearingless slice motor," *JSME Int. J. Series C*, vol. 40, pp. 593–598, 1997.

[14] D. Mazzei, F. Vozzi, A. Cisternino, G. Vozzi, and A. Ahluwalia, "A high-throughput bioreactor system for simulating physiological environments," *IEEE Trans. Ind. Electron.*, vol. 55, no. 9, pp. 3273–3280, Sep. 2008.

[15] S. S. Ozturk and W.-S. Hu, *Cell Culture Technology for Pharmaceutical and Cell-Based Therapies*. Boca Raton, FL: Taylor & Francis, 2006.

[16] J. A. Asenjo and J. C. Merchuk, *Bioreactor System Design*. New York: Marcel Dekker, Inc., 1995.

[17] K. van't Riet and J. Tramper, *Basic Bioreactor Design*. New York: Marcel Dekker, Inc., 1991.

[18] S. Ye and K. T. Chau, "Chaoization of DC motors for industrial mixing," *IEEE Trans. Ind. Electron.*, vol. 54, no. 4, pp. 2024–2032, Aug. 2007.

[19] M. A. Henson, "Biochemical reactor modeling and control," *IEEE Control Systems Magazine*, vol. 26, no. 4, pp. 54–62, Aug. 2006.

[20] G. Catapano, P. Czermak, R. Eibl, D. Eibl, and R. Pörtner, "Bioreactor Design and Scale-Up," in *Cell and Tissue Reaction Engineering: Principles and Practice*, 1st ed. vol. 1, Berlin, Germany: Springer-Verlag, 2009, pp. 173–259.

[21] G. Halász, B. Gyüre, I. M. Jánosi, K. G. Szabó, and T. Tél, "Vortex flow generated by a magnetic stirrer," *Amer. J. Phys.*, vol. 75, no. 12, pp. 1092–1098, Dec. 2007.

[22] T. Mahmud, J. A. Haque, K. J. Roberts, D. Rhodes, and D. Wilkinson, "Measurements and modeling of free-surface turbulent flows induced by a magnetic stirrer in an unbaffled stirred tank reactor," *Chem. Eng. Sci.*, vol. 64, no. 20, pp. 4197–4209, Oct. 2009.

[23] Y. Christi and M. Moo-Young, "Clean-in-place systems for industrial bioreactors: Design, validation and operation," *J. Ind. Microbiology Biotechnology*, vol. 13, no. 4, pp. 201–207, Jul. 1994.

[24] S. Silber, W. Amrhein, P. Bösch, R. Schoeb, and N. Barletta, "Design aspects of bearingless slice motors," *IEEE/ASME Trans. Mechatronics*, vol. 10, no. 6, pp. 611–617, Dec. 2005.

[25] K. Raggl, T. Nussbaumer, and J. W. Kolar, "Comparison of separated and combined winding concepts for bearingless centrifugal pumps," *J. Power Electron.*, vol. 9, no. 2, pp. 243–258, 2009.

[26] F. Zürcher, T. Nussbaumer, and J. W. Kolar, "Principles of magnetic levitation force and motor torque generation by superposition of harmonics in bearingless brushless motors," in *Proc. 35th Ann. Conf. IEEE Ind. Electron., IECON '09*, Nov. 2009, pp. 1246–1251.

[27] T. Reichert, T. Nussbaumer, W. Gruber, and J. W. Kolar, "Design of a novel bearingless permanent magnet motor for bioreactor applications," in *Proc. 35th Ann. Conf. IEEE Ind. Electron., IECON '09*, Nov., 2009, pp. 1086–1091.
[28] P. Karutz, T. Nussbaumer, W. Gruber, and J. W. Kolar, "Acceleration-performance optimization for motors with large air gaps," *IEEE Trans. Ind. Electron.*, vol. 57, no. 1, pp. 52–60, Jan. 2010.
[29] P. Karutz, T. Nussbaumer, W. Gruber, and J. W. Kolar, "Saturation effects in high acceleration bearingless slice motors," in *Proc. 2008 IEEE Int. Symp. Ind. Electron*, Jun./Jul. 2008, pp. 472–477.
[30] L. Zhu and C. R. Knospe, "Modeling of nonlaminated electromagnetic suspension systems," *IEEE/ASME Trans. Mechatronics*, vol. 15, no. 1, pp. 59–69, Feb. 2010.

Thomas Reichert (S'09) was born in Schaffhausen, Switzerland, in 1983. He received the M.Sc. degree in electrical engineering and information technology from the Swiss Federal Institute of Technology (ETH) Zurich, Zurich, Switzerland, in 2008. The focus during his studies was on mechatronics, robotics, and power systems and control. During his Master's thesis, he simulated rotor dynamics and implemented a magnetic bearing for a mega-speed drive. Since October 2008, he has been a Ph.D. student at the Power Electronic Systems (PES) Laboratory, ETH Zurich, where he is working on high-torque magnetically levitated motors.

Thomas Nussbaumer (S'02–M'06) was born in Vienna, Austria, in 1975. He received the M.Sc. degree (with honors) in electrical engineering from the University of Technology Vienna, Vienna, Austria, in 2001, and the Ph.D. degree from the Power Electronic Systems (PES) Laboratory, Swiss Federal Institute of Technology (ETH) Zurich, Zurich, Switzerland, in 2004.

From 2001 to 2006, he was with the PES Laboratory, Swiss Federal Institute of Technology (ETH) Zurich, where he conducted research on modeling, design, and control of three-phase rectifiers, power factor correction techniques, and electromagnetic compatibility. Since 2006, he has been with Levitronix GmbH, Zurich, Switzerland, where he is currently working on bearingless motors, magnetic levitation, and permanent-magnet motor drives for the semiconductor and biotechnology industry. His current research is focused on compact and high-performance mechatronic systems, including novel power electronics topologies, control techniques, drive systems, sensor technologies, electromagnetic interference (EMI), and thermal aspects.

Wolfgang Gruber (S'07–M'10) was born in Amstetten, Austria, in 1977. He received the Dipl.-Ing. degree in mechatronics and the Ph.D. degree in technical science from Johannes Kepler University, Linz, Austria, in 2004 and 2009, respectively.

He had been a Scientific Assistant at the Institute for Electric Drives and Power Electronics, Johannes Kepler University Linz, Austria, since 2004, where he was involved in teaching and various research projects. Since 2010, he holds a position as Assistant Professor at this institute. His research interests include magnetic bearings, bearingless motors, and brushless motors.

Prof. Gruber is a member of the Association for Electrical, Electronic and Information Technologies (VDE).

Johann W. Kolar (M'89–SM'04–F'10) received the Ph.D. degree *(summa cum laude/promotio sub auspiciis praesidentis rei publicae)* from the University of Technology Vienna, Vienna, Austria.

Since 1984, he had been working as an Independent International Consultant in close collaboration with the University of Technology Vienna, in the fields of power electronics, industrial electronics, and high performance drives. He has proposed numerous novel PWM converter topologies, and modulation and control concepts, e.g., the VIENNA Rectifier and the Three-Phase AC-AC Sparse Matrix Converter. He has published more than 300 scientific papers in international journals and conference proceedings and has filed more than 75 patents. He was appointed Professor and Head of the Power Electronic Systems Laboratory at the Swiss Federal Institute of Technology (ETH) Zurich, Zurich, Switzerland, on Feb. 1, 2001. The focus of his current research is on ac-ac and ac-dc converter topologies with low effects on the mains, e.g., for power supply of telecommunication systems, More-Electric-Aircraft, and distributed power systems in connection with fuel cells. Further main areas are the realization of ultra-compact intelligent converter modules employing latest power semiconductor technology (SiC), novel concepts for cooling and EMI filtering, multidomain/multiscale modeling and simulation, pulsed power, bearingless motors, and Power MEMS.

Prof. Kolar is a member of the IEEJ and of Technical Program Committees of numerous international conferences in the field (e.g., Director of the Power Quality Branch of the International Conference on Power Conversion and Intelligent Motion). He received the Best Transactions Paper Award of the IEEE Industrial Electronics Society in 2005. He also received an Erskine Fellowship from the University of Canterbury, New Zealand, in 2003. In 2006, the European Power Supplies Manufacturers Association (EPSMA) awarded the Power Electronics Systems Laboratory of ETH Zurich, as the leading academic research institution in Europe. From 1997 through 2000, he has been serving as an Associate Editor of the IEEE TRANSACTIONS ON INDUSTRIAL ELECTRONICS, and since 2001, as an Associate Editor of the IEEE TRANSACTIONS ON POWER ELECTRONICS. Since 2002, he is also an Associate Editor of the *Journal of Power Electronics* of the Korean Institute of Power Electronics and a member of the Editorial Advisory Board of the *IEEJ Transactions on Electrical and Electronic Engineering*.